01 Jan 2006

Regulation of Powder Mass Flow Rate in Gravity-Fed Powder Feeder Systems

Vishnu Thayalan

Robert G. Landers
Missouri University of Science and Technology, landersr@mst.edu

Regulation of Powder Mass Flow Rate in Gravity–Fed Powder Feeder Systems

Vishnu Thayalan and Robert G. Landers

University of Missouri–Rolla

Department of Mechanical Engineering

1870 Miner Circle, Rolla, Missouri 65409–0050

{vishnu,landersr}@umr.edu

ABSTRACT

Precise regulation of powder mass flow in laser based manufacturing processes is critical to achieving excellent part dimensional and microstructure quality. Control of powder mass flow in laser based manufacturing processes is challenging since low flow rates, where nonlinear effects are significant, are typically required. Also, gravity–fed powder feeder systems have significant material transport delays, making the control of powder mass flow even more challenging. This paper presents a control strategy for regulating the powder mass flow rate in a gravity–fed powder feeder system. A dynamic model of the powder feeder system, including material transport delay, is constructed and a modified proportional plus integral (PI) controller is designed. An observer is used to estimate powder mass flow rate using the powder feeder motor encoder signal. The control strategy is implemented in a Smith Predictor Corrector Structure, which has been adjusted such that it can be applied to the modified PI controller, to account for

the inherent material transport delay. Experimental studies are conducted that validate the dynamic model and controller strategy.

KEYWORDS

Gravity–fed powder feeders, powder mass flow regulation, delay control, laser aided manufacturing

INTRODUCTION

Powder mass flow rate is a crucial input to laser based manufacturing applications. An example of one such application is laser metal deposition (see Figure 1). Part geometry quality, in terms of dimensional accuracy, is directly related to the rate at which raw material is supplied to the work zone. Further, the part microstructure characteristics (e.g., porosity, surface finish) is directly related to powder mass flow rate. It is typically desirable to maintain a constant flow rate to create uniform deposition. Laser based applications are often low powder mass flow rate processes (typically on the order of 5–20 g/min), making powder mass flow rate difficult to sense and control.

Powder delivery systems fall into two major classifications: fluidized bed and mechanical delivery systems. Fluidized bed systems utilize a fluidizing stream to agitate the powder and a carrier gas to transport the powder. As the particles are transported by a pneumatic conveyor, the pressure drop across the conveying tube is compared to the pressure drop due to pure air flow.

Additional pressure drop is proportional to the powder mass being transported. The measurement systems of such powder feeder devices use an orifice meter and pressure transducers to indirectly measure powder mass flow rate. Mechanical powder feeders use a hopper, a delivery system, and a measuring device. The measurement devices are optical, electrostatic, or electromagnetic sensors to sense powder mass flow rate.

One of the biggest obstacles to controlling powder mass flow rate in laser based manufacturing processes lies in continuous real–time measurement. As Hannon [2000] reported, for low flow applications, there are few practical methods to measure powder mass flow online. Huang *et al.* [2001] used pressure and temperature transducers to determine the flow drop across the conveying tube. Powder mass flow rate was calculated from the pressure drop and powder concentration. Similar measurement systems were developed by Tardos *et al.* [1996] to quantify the quality of powder mixing in crystallization applications. The feeder was a vibratory feeder (mechanical system) with a weight sensing device to detect flow rate. Optical sensors measured the intensity loss from a light beam when it was directed though a powder stream. Greater flow rates resulted in greater intensity loss, generating a change in sensor feedback. Hannon [2000] used the attenuation of a laser beam to measure powder mass flow rate. Powder mass flow during a finite time was collected and weighed using a strain gage coupled to a weighing scale to validate the method.

For an automobile coating application, Moses [1995] used load cells to estimate powder mass flow from a hopper to control the coating thickness. If powder mass flow was different than required powder mass flow rate for a particular thickness, pneumatic valves were adjusted.

Acoustic control of powder mass flow was used by Yang and Evans [2003] to regulate powder mass flow for a solid free forming application. Acoustic control, a variation of vibratory feeding, was accomplished through forced vibration of tubes delivering powder. The tubes were vibrated by a sub–woofer loudspeaker and powder mass flow was measured by a balance. Experimental studies revealed that powder mass flow rate varied inversely as the frequency of the forcing waveform. Yanagida *et al.* [2000] used a capacitance sensor with a fluidized powder feeder system to detect electrostatic changes due to variation in powder mass flow. The sensor feedback was sent to a PLC, which used calibrated tables to send appropriate control inputs to pneumatic regulators.

As part of the development of an automated workstation for laser alloy cladding, Carvalho *et al.* [1995] modified an existing commercial powder feeder for closed–loop control. Powder mass flow rate was measured from the speed of a metering wheel, which was driven by a motor. Calibration functions relating the powder size and bulk density were used to correlate mass flow rate to the wheel velocity. Since each powder is different, these functions had to be recomputed whenever the powder was changed. A PC with plug–in DAQ cards was used to perform data acquisition and control. However, no systematic technique was used to control the powder flow.

Li and Steen [1993] developed a pressure–based sensor for continuous powder mass flow rate measurement and control. Pressure difference across a delivery tube acted upon a silicon chip in the sensor, which generated a corresponding voltage. A dynamic model of the mass flow rate was obtained from an analysis of the driving screw mechanism and the pneumatic conveying process. A feedforward control strategy was used to attain the reference flow rate, and controller

performance with stainless steel powder was demonstrated. However, no systematic technique was used to design the control system and the material transport delay was ignored.

This paper presents a mechanistic dynamic model of powder mass flow rate in mechanical gravity–fed powder feeder systems. The model combines an analytical servomechanism model and an empirical model of the dynamics induced by the delivery structure. Powder mass flow rate is estimated based on the motor velocity observed from motor encoder data and the system model. The mechanistic dynamic model allows the control engineer to select control gains systematically to achieve desired system performance. The control system performance is verified via a set of experimental studies.

POWDER FEEDER SYSTEM DESCRIPTION

This section describes the gravity–fed powder feeder system that will be used in all subsequent experimental studies. The powder feeder system schematic is shown in Figure 2. The powder feeder system has two hoppers, each with a separate sensing and actuation system. Powder is stored in both hoppers, which are placed above the delivery system. Helical screws, driven by motors, push powder through the barrels and into a mixer, from which it flows into the splitter tubes. The tubes direct the powder to the nozzle where it flows coaxially with the laser by an inner and outer argon gas system. The inner gas protects the nozzle from hot gases resulting during laser–metal interaction. The outer gas acts as a shield, protecting the part from oxidation. From the nozzle, the powder is delivered to the substrate.

Each hopper has the same sensing and actuation system; namely, a motor with an embedded encoder. The motors are internally geared and rated at 24 V DC. The motors are equipped with 3 channel encoders attached to the motor shafts. Each motor is driven by a separate pulse width modulated (PWM) servo amplifier. The amplifier gain can be adjusted by an onboard potentiometer, and is set to a gain of 2.46 such that the full range of the analog output device can be utilized. The motor specifications are given in Table 1. The motor output shaft is connected to the hopper screw through a direct drive (i.e., 1:1) gear system. The rotational encoders, which are mounted on the motor shafts, have 3 feedback channels, with a line count of 500 counts/revolution. By counting signals on the auxiliary encoder feedback channels (called X4 encoding), the line count is effectively increased to 2000 counts/revolution, providing an angular displacement resolution of 0.0126 *rad*. For the experiments conducted in this paper, an optical sensor, which is fixed to the nozzle, is used as a direct measurement of powder mass flow rate at the nozzle. The device consists of a receiver and a transmitter. When powered, the transmitter emits a light beam, which is collected by the receiver. If the light beam is blocked by an object, the sensor returns a voltage proportional to the blocking object's opacity. In a laser metal deposition operation, the optical sensor cannot be used to measure the powder mass flow rate at the nozzle since the laser beam will interfere with the optical sensor. Therefore, the encoder will be utilized to provide an indirect method of estimating powder mass flow rate at the nozzle.

A National Instruments real–time data acquisition and control system is used to interface the sensors and actuators to the chassis and consists of three components: a multifunction board (PXI 6040E) to acquire analog inputs, a counter/timer board (PXI 6602) to acquire digital encoder signals, and an analog output board (PXI 6711) to send the control voltage to the motor. The

multifunction board has eight analog input channels, each with a range of ±10 *V* and 12 bits providing a resolution of 4.88 *mV*. The analog output board has eight analog output channels, each with a range of ±10 *V* and 12 bits for a resolution of 4.88 *mV*. The counter/timer board has eight counters and 100 *kHz* or 20 *MHz* internal time bases for counting/timing operations. The boards are capable of sending and receiving TTL signals through backplane connectors or by external wiring, allowing for flexible timing and synchronization. An overview of the data acquisition timing scheme is shown in Figure 3. Hardware configurations such as buffer settings, sampling clock speed, and buffer size are set in the control software program, allowing for proper timing and synchronization. The program is then downloaded to a National Instruments PXI 8170 real–time controller running Labview Real Time 6.1®. Data from the real–time controller is transferred to a PC interfaced to the real–time controller by a 10 MBPS Ethernet cable.

DYNAMIC SYSTEM MODEL

A control–oriented, dynamic model of the powder feeder system is constructed by modeling its individual components. A complete dynamic model of the powder feeder system considered in this paper was given in Pan *et al*. [2005] and is summarized below. The motor position is related to the screw angular velocity by

$$\dot{\theta}_m(t) = K_s \omega_s(t) \tag{1}$$

where $\theta_m(t)$ is the motor angular displacement (*rad*), K_s is the motor internal gear ratio, and $\omega_s(t)$ is the screw angular speed (*rad*/*s*). The motor current (*A*) is

$$I(t) = \frac{K_a}{R} V_c(t) - \frac{K_v}{R} \omega_m(t) \tag{2}$$

where K_a is the amplifier gain, R is the motor electrical resistance (Ω), $V_c(t)$ is the control voltage (V), K_v is the motor velocity constant ($V/(rad/s)$), and $\omega_m(t)$ is the motor angular speed (rad/s). Summing the torques applied to the motor shaft

$$J_m \dot{\omega}_m(t) = -B_m \omega_m(t) + K_t I(t) - T_f \operatorname{sgn}\left(\omega_m(t)\right) \tag{3}$$

where J_m is the motor mass moment of inertia ($kg{\cdot}m^2$), B_m is the motor viscous damping coefficient ($N{\cdot}m{\cdot}s$), K_t is the motor torque constant ($N{\cdot}m/A$), and T_f is the motor Coulomb torque magnitude ($N{\cdot}m$). The screw speed is related to the motor speed by

$$\omega_s(t) = K_s \omega_m(t) \tag{4}$$

Given the small internal motor gear gain (i.e., $K_S = 218.4^{-1}$) used to achieve low powder mass flow rates, the screw inertia and friction can be ignored. The hopper powder mass flow rate is related to the screw speed by

$$m_h(t) = \begin{cases} 0 & \text{if} \quad \omega_s(t) \le 0 \\ K_{flow}\omega_s(t) & \text{if} \quad \omega_s(t) > 0 \end{cases} \tag{5}$$

where $m_h(t)$ is the hopper powder mass flow rate (g/min) and the K_{flow} is the flow rate–screw velocity gain ($(g/min)/(rad/s)$) and has a value of 15.3 (g/min)/(rad/s), assuming the material density is density 7200 kg/m^3. This parameter was determined by empirical correlations. The powder mass flow rate at the nozzle is related to the hopper mass flow rate by

$$\tau_p \dot{m}_n(t) + m_n(t) = m_h(t - T_d) \tag{6}$$

where $m_n(t)$ is the powder mass flow rate at the nozzle (g/min) and T_d is the powder mass flow rate delay period (sec). The powder feeder system time constant is $\tau_p = 0.265$ sec and the time delay is $T_d = 1.71$ sec. Both parameters were determined via detailed simulation studies [Pan *et al*., 2006], which utilized Discrete Particle Modeling (DPM). Given an empirical distribution of the size and shape of the powder particles utilized in the experiments and the powder delivery

system geometry, including such details and the size, orientation, and number of tubes, simulation studies involving thousands of particles were conducted to determine the powder feeder delivery system dynamic characteristics. The modeling included powder dispersion in the powder delivery system induced by non–spherical particle–wall collisions and three–dimensional friction collision to simulate the interactions between particles and the powder delivery system walls. Ignoring the nonlinearity in equation (5), the flow rate at the nozzle is related to the control voltage and Coulomb friction force in the Laplace domain by

$$m_n(s) = \frac{K_c K_{flow} e^{-T_d s}}{(\tau_m s + 1)(\tau_p s + 1)} V_c(s) - \frac{K_f K_{flow} e^{-T_d s}}{(\tau_m s + 1)(\tau_p s + 1)} T_f(s) \tag{7}$$

where $K_c = \frac{K_s K_a K_t}{B_m R + K_t K_v}$ is the screw speed–voltage gain ((*rad*/*s*)/*V*), $K_f = \frac{K_s R}{B_m R + K_t K_v}$ is the screw speed–disturbance torque gain ((*rad*/*s*)/*N*·*m*), and $\tau_m = \frac{J_m R}{B_m R + K_t K_v}$ is the motor mechanical time constant (*sec*). Note that the powder feeder delivery system dynamics depend the powder mass, size and shape distribution, etc. Therefore, the model must be updated for different powder mixtures. For different lots of the same powder this change is typically negligible; however, for a different powder material, substantially different powder size, or drastic changes in the environmental conditions (e.g., humidity) the flow rate–screw velocity gain, powder feeder system time constant, and powder feeder system time delay will need to be recalculated.

Model Validation

The developed mechanistic powder feeder system model is verified by conducting two open–loop tests and comparing the simulation and experimental results. Note that these tests consist of

experimental data that was not used to develop the model. The first test consists of a series of step control voltages given to the motor amplifier. The resulting control voltage, measured output, and simulated output signals are shown in Figure 4. Visually, the measured and simulated output signals cannot be distinguished. To qualitatively compare the signals, the following goodness of fit parameter is employed

$$\gamma = \sqrt{\frac{\sum_{i=1}^{N_s}\left[m_s(i) - \bar{m}_n\right]^2}{\sum_{i=1}^{N_s}\left[m_n(i) - \bar{m}_n\right]^2}} \tag{8}$$

where N_s is the number of data points, m_s is the simulated powder mass flow rate at the nozzle (g/min), and $\bar{m}_n$ is the average powder mass flow rate at the nozzle (g/min). A value of 1 denotes a perfect model. Note that the goodness of fit parameter must be positive and can be less than or greater than 1.

The goodness of fit parameter for the data in Figure 4 is 0.9993, indicating an excellent fit. In a validation test, a white noise control voltage signal (i.e., a series of control voltages randomly distributed between 0 and 10 V with a mean of 5 V and a Gaussian distribution) is input to the motor amplifier. The resulting control voltage, measured output, and simulated output signals are shown in Figure 5. Again, the measured and simulated output signals cannot be distinguished visually. The goodness of fit parameter for this case is 1.0054. These results demonstrate that the mechanistic powder feeder system model is an excellent dynamic representation of the true system.

CONTROL STRATEGY

A control strategy is now designed to regulate the powder mass flow rate in gravity–fed powder feeder systems. The controller will be designed such that it can reject constant disturbances, such as Coulomb friction, and track constant powder mass flow rate commands. The control strategy consists of the following components:

1. ***Control Algorithm*:** A modified proportional plus integral (PI) controller is utilized. The controller will reject constant disturbances and robustly track constant powder mass flow rate commands.
2. ***Smith Predictor Corrector Structure (SPCS)*:** Since gravity–fed powder feeder systems naturally contain material transport delays, the controller will be implemented in the SPCS to ensure stability and performance. The SPCS is adjusted such that it can be applied to the modified PI controller.
3. ***Nozzle Powder Mass Flow Rate Estimator*:** Since the powder mass flow rate at the nozzle cannot be directly measured during the laser metal deposition process, it is estimated using actuator measurements.

A complete block diagram of the closed–loop system is shown in Figure 6. The control strategy is implemented for the powder feeder system described above.

Controller Design

The motor dynamics are ignored in the controller design since $\tau_m \ll \tau_p$. A system model in the digital domain is determined by applying a zero order hold with a sample period of $T = 10$ *ms*. Therefore, the digital model used for controller design is

$$\frac{m_n(z)}{V_c(z)} = \frac{K_z}{z + a_p} z^{-n_p} = \frac{0.135}{z - 0.963} z^{-171} \tag{9}$$

where z is the discrete time forward shift operator, $n_p = \frac{T_d}{T}$ is the number of delay samples, $a_n = -e^{-\frac{T}{\tau_p}}$ is the powder delivery system digital open–loop pole, and $K_z = K_c K_{flow}(1+a_p)$ is the digital powder delivery system mass flow rate–voltage gain ((*g*/*min*)/*V*). A controller is now designed ignoring the delay and subsequently will be implemented in a Smith Predictor–Corrector structure, which has been adjusted such that it can be applied to the modified PI controller, to explicitly account for the delay. The control law, ignoring the delay, is

$$V_c(z) = K_i T \frac{z}{z-1} E(z) - K_p M_n(z) \tag{10}$$

where K_i is the controller integral gain (*V*·*s*/(*g*/*min*)), E is the nozzle powder mass flow rate error (*g*/*min*), and K_p is the controller proportional gain (*V*/(*g*/*min*)). This is a modified Proportional plus Integral (PI) controller, whose P term operates on the negative of the feedback signal instead of the error. The modified PI controller has an advantage over the conventional PI controller in that the closed–loop zeros are guaranteed to be stable, provided the open–loop zeros are stable. The nozzle powder mass flow rate error is defined as

$$E(z) = M_r(z) z^{n_p} - M_n(z) \tag{11}$$

where M_r is the reference powder mass flow rate at the nozzle(g/min). The reference is shifted n_p samples ahead to account for the powder material transport delay. The closed–loop transfer function, ignoring the delay, is

$$\frac{M_n(z)}{M_r(z)} = \frac{K_z K_i z}{z^2 + \left(a_p - 1 + K_z K_i T + K_z K_p\right) z - \left(a_p + K_z K_p\right)} \tag{12}$$

For desired closed–loop time constants of τ_1 (sec) and τ_2 (sec), the desired closed–loop characteristic equation is

$$z^2 + \left(e^{-T/\tau_1} + e^{-T/\tau_2}\right) z + e^{-T/\tau_1} e^{-T/\tau_2} = z^2 + \alpha_1 z + \alpha_0 = 0 \tag{13}$$

Therefore, the proportional and integral gains, respectively, are

$$K_p = \frac{-\alpha_0 - a_n}{K_z} \tag{14}$$

$$K_i = \frac{\alpha_1 + 1 - a_n - K_p K_z}{T K_z} \tag{15}$$

Smith Predictor Corrector Structure (SPCS)

The powder feeder system material transport delay must be taken into account when implementing the controller; otherwise, instability may occur. If the material transport delay is not taken into account, then performance must be drastically sacrificed to maintain closed–loop stability. An effective method to compensate for delays is to implement the compensator in a Smith–Predictor Corrector Structure (SPCS). The SPCS consists of the common feedback loop and an inner loop that introduces two new terms into the feedback path. The ‘predictor’ term predicts the powder mass flow rate using the system model, and the ‘corrector’ term is an estimate of the powder mass flow rate without the delay. The ‘predictor’ term cancels the measurement and the controller operates on the ‘corrector’ term. Since the ‘corrector’ term is

linear and does not contain a delay, linear control designs may be utilized. The 'predictor' and 'corrector' terms modify the feedback to the controller such that closed–loop stability and performance are ensured.

In the SPCS, the SPCS error term is

$$e_1(k) = -a_p e_1(k-1) + K_z\left(V_c(k-1) - V_c\left(k-1-n_p\right)\right) - K_{fz}\left(T_f(k-1) - T_f\left(k-1-n_p\right)\right) \quad (16)$$

where $e_1(k)$ is the SPCS error term (g/min) and $K_{fz} = K_f K_{flow}(1+a_p)$ is the digital screw speed–disturbance torque gain ($(rad/s)/N{\cdot}m$). The signal $e_1(k)$ is the difference between an estimate of the system without the delay and an estimate of the system with the delay. For a controller that only operates on the system error signal (e.g., a conventional PI controller) the SPCS error term is subtracted from the error signal and the controller operates on the resulting signal, $e(k) - e_1(k)$, in place of the error signal. However, for the modified PI controller utilized in this paper, the integral term operates on the signal $e(k) - e_1(k)$ and the proportional term operates on the signal $m_n(k) + e_1(k)$, making the closed–loop system characteristic equation independent of the inherent system delay. This is proved in the Appendix. Therefore, the command voltage is

$$V_c(k) = V_c(k-1) + K_i T\left[e(k) - e_1(k)\right] - K_p\left[m_n(k) + e_1(k)\right] + K_p\left[m_n(k-1) + e_1(k-1)\right] \quad (17)$$

Anti integral windup and command voltage saturation are both implemented in the control algorithm.

Nozzle Powder Mass Flow Rate Observer

The technology does not currently exist to reliably obtain a direct measurement of the powder mass flow rate at the nozzle in laser–aided manufacturing operations. This would typically lead one to use a measurement–based observer to estimate the powder flow rate; however, it can be

shown that the powder mass flow rate at the nozzle is not directly observable from the system measurements. Therefore, a two–step estimation routine is utilized. First, a measurement–based observer is constructed to estimate the screw angular speed from motor angular position measurements. Next, the screw angular speed estimate is input into the model in equations (5) and (6) to estimate the powder mass flow rate at the nozzle. It should be noted that the second estimate is a purely model–based estimate whose accuracy will suffer from model uncertainties, parameter variations, and disturbances that act directly on the powder flow rate at the nozzle. However, since the powder flow rate is unobservable from the system measurements and the technology does not exist to reliability measure the powder flow rate at the nozzle directly during laser–based manufacturing operations, the hybrid measurement/model–based estimator outlined below is utilized.

The motor dynamics, given by equations (1)–(4), are transformed into the digital domain using a zero order hold equivalent. The state–space motor dynamic equations used for designing the screw angular speed measurement–based observer are

$$\begin{bmatrix} \theta_m(k) \\ \omega_s(k) \end{bmatrix} = \begin{bmatrix} 1 & \frac{T}{K_s} \\ 0 & -a_m \end{bmatrix} \begin{bmatrix} \theta_m(k-1) \\ \omega_s(k-1) \end{bmatrix} + \begin{bmatrix} 0 \\ 1 \end{bmatrix} u(k-1) \tag{18}$$

where $a_m = \exp(-T/\tau_m)$ is motor mechanical digital open–loop pole and

$$u(k) = K_c(1+a_m)V_c(k) - K_f(1+a_m)T_f(k) \tag{19}$$

Using reduced order linear estimation techniques, the estimated screw angular velocity is

$$\hat{\omega}_s(k) = L_\omega \theta_{meas}(k) + Q(k) \tag{20}$$

where $\hat{\omega}_s(k)$ is the estimated screw angular speed (*rad*/*s*), $\theta_{meas}(k)$ is the measured motor angular position (*rad*) and

$$Q(k) = F_\omega Q(k-1) + \bar{G}_\omega \theta_{meas}(k-1) + H_\omega u(k-1) \tag{21}$$

The estimator parameters are calculated such that the observer pole has a time constant of τ_e (*sec*). Since the powder mass flow rate at the nozzle is unobservable, it is estimated using the digital implementation of equations (5) and (6)

$$\hat{m}_n(k) = -a_p \hat{m}_n(k-1) + K_{flow}(1+a_p)\hat{\omega}_s(k-1-n_p) \tag{22}$$

where $\hat{m}_n(t)$ is the estimated powder mass flow rate at the nozzle (*g*/*min*). This estimate is purely model–based and will directly depend on the accuracy of the model. Further, the model must be updated for new powder mixtures since it highly depends on powder mass, size and shape distribution, etc.

EXPERIMENTAL STUDIES

The controller is experimentally implemented for H–13 tool steel powder: density 7200 kg/m^3. The desired controller time constants are τ_1 = 0.1 *sec* and τ_2 = 0.09 *sec* and the controller gains are $K_p = 1.11\frac{V}{(g/min)}$ and $K_i = 7.25\frac{V \cdot s}{(g/min)}$. The estimator parameters are calculated such that the observer pole has a time constant of 0.01 *sec*, which is significantly faster than the controller poles, and are L_ω = –0.0148, H_ω = 1, F_ω = 0.368, and $\bar{G}_\omega = 0.00935$.

Open–Loop Control

Many powder feeder systems are implemented in an open–loop (feedforward) configuration where a constant input is supplied to the actuating mechanism. The corresponding powder mass flow rate is typically determined from an empirical correlation between actuator input and steady–state powder mass flow rate measurements. However, open–loop control suffers from model uncertainties, parameter variations, and unknown disturbances that act on the system. For example, mechanical parts will wear over time and the disturbance torque acting on the motor will change depending on how much powder is left in the hopper and how it is concentrated around the screw. In the first experimental study, a constant voltage is input to the motor amplifier to achieve a powder mass flow rate of 5 *g*/*min*. The voltage magnitude is determined using the mechanistic model developed above and is $5/(K_c K_{flow}) = 1.34\ V$. The resulting control voltage and reference and actual powder mass flow rate signals are shown in Figure 7. In this case the actual powder mass flow rate does not track the reference powder mass flow rate of 5 *g*/*min*. This tracking error is mainly due to the amplifier nonlinearity in the low voltage range [Thayalan and Landers, 2004]. Therefore, measurement feedback is required to reduce the tracking error.

Controller not Implemented in SPCS

Powder feeder control systems reported in the literature do not explicitly account for the inherent material transport delay. If the delay is ignored, the system speed of response must be slow if the closed–loop system is to be stable. Otherwise, if one seeks to increase system performance, the closed–loop system will, at some point, become unstable. For the next experiment, the PI controller described above is utilized with a reference mass flow rate of 5 *g*/*min*; however, the

controller is not implemented in the SPCS. The resulting control voltage and reference and actual powder mass flow rate signals are shown in Figure 8. The closed–loop system enters an unstable limit cycle where the control voltage alternately saturates at the upper and lower limits. This instability is due to the fact that the substantial delay period was ignored and causes an uncontrolled powder mass flow rate where it rises to a large value, becomes zero, rises to a large value, etc. The results of this experimental study indicate the importance of implementing the controller in the SPCS to account for the powder feeder system material transport delay.

Controller Implemented in SPCS

To account for the material transport delay in the powder feeder system, the controller is implemented in a SPCS, which has been adjusted such that it can be applied to the modified PI controller. Four experimental studies are conducted where the reference powder mass flow rates are 5, 10, 15, and 20 *g*/*min*, respectively, and the resulting control voltage and reference and actual powder mass flow rate signals are shown in Figures 9, 10, 11, and 12, respectively. In each case there is zero steady–state error. The dynamic response is overdamped and approximately five times faster than the open–loop response. The control voltage has a slight spike every delay period (i.e., 1.71 *sec*) that causes a slight increase in the powder mass flow rate. These slight spikes are due to the fact that the control voltage is a function of its past values; namely, 1.71 *sec* in the past. However, these spikes damp out after two cycles. Note that the speed of response could be increased slightly; however, the increase is limited by control voltage saturation and the magnitude of the control voltage spikes every delay period would increase.

The last experimental study involves several step tests over the operating range of the powder feeder system considered in this paper. The resulting control voltage and reference and actual powder mass flow rate signals are shown in Figure 13. Again, the control system provides an overdamped response that is approximately five times faster than the open–loop response. By feeding the reference forward, the control voltage is automatically adjusted before the next reference signal occurs to avoid a delay in the powder mass flow rate output signal. The controller is able to provide a consistent dynamic response over the entire operating range of the powder feeder system.

SUMMARY AND CONCLUSIONS

This paper presented a mechanistic powder feeder system model, an approach for the indirect measurement of powder mass flow rate in gravity–fed mechanical powder feeder systems based on motor encoder data, and a powder mass flow rate control system that directly accounts for the inherent material transport delay. The controller was a modified Proportional plus Integral (PI) controller where the proportional term operated on the negative of the sensor signal, instead of the error. A Smith Predictor–Corrector Structure was utilized to directly account for the material transports delay and was adjusted such that it can be utilized by the modified PI controller. Experimental studies were conducted that demonstrated the need to control gravity–fed powder feeder systems and account for the material transport delay. Further experimental studies, conducted over the operating range of a powder feeder system, validated the dynamic model and control strategy. The major contribution of this paper is that for the first time a complete dynamic model of a gravity–fed powder feeder system, including the material transport delay,

was used to systematically design a controller that directly accounted for this delay and regulated the powder flow rate at a constant value. Systematic control design allows for a more cost–effective design process that does not have to resort to a multitude of trial and error tests on the experimental system. Also, directly accounting for the inherent material transport delays allows the designer to create a closed–loop system with a faster response that is more robust to possible disturbances.

ACKNOWLEDGEMENTS

The authors gratefully acknowledge the financial support of the National Science Foundation (DMI–9871185), Society of Manufacturing Engineers (#02022–A), Missouri Research Board, and the Intelligent Systems Center at the University of Missouri–Rolla.

APPENDIX

In this section it is proved that, for the modified PI controller applied to general linear systems with delays, if the proportional term operates on the signal $y(k) + e_1(k)$, the closed–loop characteristic equation will be independent of the system delay. The plant dynamics are

$$Y(z) = G_p(z)U(z)z^{-d} - G_d(z)D(z)z^{-d} \tag{23}$$

where $Y(z)$ is the plant output, $G_p(z)$ is the plant transfer function, $U(z)$ is the plant input, d is the number of delay samples, $G_d(z)$ is the disturbance transfer function, and $D(z)$ is the disturbance. The error and SPCS error terms, respectively, are

$$E(z) = R(z)z^{d} - Y(z) \tag{24}$$

$$E_1(z) = G_p(z)U(z)\left[1 - z^{-d}\right] - G_d(z)D(z)\left[1 - z^{-d}\right] \tag{25}$$

where $R(z)$ is the reference signal. The control law when implementing the modified PI controller in the proposed SPCS is

$$U(z) = -K_p\left[Y(z) + E_1(z)\right] + K_i\frac{z}{z-1}\left[E(z) - E_1(z)\right] \tag{26}$$

Combining equations (23)–(26)

$$Y(z)\left[z - 1 + K_pG_p(z-1) + K_iG_pz\right] = K_iG_pzR(z) - G_dD(z)(z-1)z^{-d} \tag{27}$$

From equation (27) the closed–loop characteristic equation is

$$z - 1 + K_pG_p(z-1) + K_iG_pz = 0 \tag{28}$$

which is independent of the inherent system delay.

NOMENCLATURE

a_m Motor mechanical digital open–loop pole [–0.336]

a_p Powder delivery system digital open–loop pole [–0.963]

B_m Motor viscous damping coefficient [$2.6\cdot10^{-6}$ $N\cdot m\cdot s$]

e Nozzle powder mass flow rate error [g/min]

e_1 SPCS error term [g/min]

I Motor current [A]

I_{max} Maximum motor current [A]

I_{min} Minimum motor current [A]

J_m Motor mass moment of inertia [$4.2\cdot10^{-6}$ $kg\cdot m^2$]

k Sample iteration

K_a Amplifier gain [2.46]

K_c Screw speed–voltage gain [0.24 $(rad/s)/V$]

K_f Screw speed–disturbance torque gain [10 $(rad/s)/N{\cdot}m$]

K_{flow} Flow rate–screw velocity gain [15.3 $(g/min)/(rad/s)$]

K_{fz} Digital screw speed–disturbance torque gain [6.65 $(rad/s)/N{\cdot}m$]

K_i Controller integral gain [$V{\cdot}s/(g/min)$]

K_p Controller proportional gain [$V/(g/min)$]

K_s Motor internal gear ratio [216.4^{-1}]

K_t Motor torque constant [$4.59{\cdot}10^{-2}$ $N{\cdot}m/A$]

K_v Motor voltage constant [$4.59{\cdot}10^{-2}$ $V/(rad/s)$]

K_z Digital powder delivery system mass flow rate–voltage gain [0.135 $(g/min)/V$]

m_h Hopper powder mass flow rate [g/min]

m_n Powder mass flow rate at the nozzle [g/min]

$\hat{m}_n$ Estimated powder mass flow rate at the nozzle [g/min]

$\bar{m}_n$ Average powder mass flow rate at the nozzle [g/min]

m_r Reference powder mass flow rate at the nozzle [g/min]

m_s Simulated powder mass flow rate at the nozzle [g/min]

n_p Number of delay samples [171]

N_s Number of samples in a data set

R Motor electrical resistance [4.62 Ω]

s Laplace variable

t Time [sec]

T_d Powder mass flow rate delay period [1.71 *sec*]

T_f Motor Coulomb torque magnitude [$4.2 \cdot 10^{-3}$ $N \cdot m$]

T Sample period [10 *ms*]

V_c Control voltage [*V*]

z Discrete time forward shift operator

γ Goodness of fit parameter

θ_m Motor angular position [*rad*]

θ_{meas} Measured motor angular position [*rad*]

$\dot{\theta}_m$ Motor angular speed [*rad*/*s*]

τ_m Motor mechanical time constant [0.0092 *sec*]

τ_p Powder delivery system time constant [0.265 *sec*]

$\tau_{1,2}$ Controller desired time constants [*sec*]

ω_m Motor angular speed [*rad*/*s*]

$\dot{\omega}_m$ Motor angular acceleration [rad/s^2]

ω_s Screw angular speed [*rad*/*s*]

$\hat{\omega}_s$ Estimated screw angular speed [*rad*/*s*]

REFERENCES

Carvalho, P.A., Braz, N., Pontinha, M.M., Ferreira, M.G.S., Steen, W.M., Vilar, R., and Watkins, K.G., 1995, "Automated Workstation for Variable Composition Laser Cladding – Its Use for Rapid Alloy Scanning," *Surface and Coatings Technology*, Vol. 72, pp. 62–70.

Hannon, K.M., 2000, "Preliminary Development of a Real–Time Powder Mass Flow Controller and Feeder for Powder Welding Applications," M.S. Thesis, Department of Mechanical Engineering, University of North Carolina, Charlotte, NC.

Huang, Z., Wang, B., and Li, H., 2001, "An Intelligent Measurement System for Powder Mass Flowrate Measurement in Pneumatic Conveying System," *IEEE Instrumentation and Measurement Technology Conference*, Budapest, Hungary, May 21–23, pp. 1237–1240.

Li, L. and Steen, W.M., 1993, "Sensing, Modeling and Closed–Loop Control Of Powder Feeder for Laser Surface Modification," *ICALEO*, pp. 964–974.

Moses, D.L., 1995, "Powder Mass Flow Control for Automotive Systems," Technical Paper, *SME Finishing Conference*, Cincinnati, Ohio, September 18–21, pp. FC95–249–1–7.

Landers, R.G., Pan, H., and Liou, F., 2006, "Dynamic Modeling of Powder Delivery Systems in Gravity–Fed Powder Feeders," *ASME Journal of Manufacturing Science and Engineering*, Vol. 128, No. 1 (to appear).

Tardos, G. and Lu, Q., 1996, "Precision Dosing of Powders by Vibratory and Screw Feeders: an Experimental Study," *Advanced Powder Technology*, Vol. 7, No. 1, pp. 51–58.

Thayalan, V. and Landers, R.G., 2004, "Control of Powder Mass Flow Rate in Laser Metal Deposition Processes," *ASME International Mechanical Engineering Congress and Exhibition*, Anaheim, California, November 13–19 (on CD ROM).

Yanagida, K., Morita, T., and Takeuchi, M., 2000, "A New Powder Mass Flow Control System for Electrostatic Powder Coating: A Closed–Loop Control System Equipped with a Capacitance Sensor," *Journal of Electrostatics*, Vol. 49, No. 1, pp. 1–13.

Yang, S. and Evans, J.R.G., 2003, "Computer Control of Powder Mass Flow for Solid Freeforming by Acoustic Modulation," *Powder Technology*, Vol. 133, No. 1–3, pp. 251–254.

Table 1: Powder Feeder Motor Specifications.

Parameter	Symbol	Units	Value
Voltage Constant	K_v	$V/(rad/s)$	$4.59 \cdot 10^{-2}$
Torque Constant	K_t	$N \cdot m/A$	$4.59 \cdot 10^{-2}$
Electrical Resistance	R	Ω	4.62
Mechanical Inertia	J_m	$kg \cdot m^2$	$4.2 \cdot 10^{-6}$
Viscous Damping	B_m	$N \cdot m \cdot s$	$2.6 \cdot 10^{-6}$
Coulomb Friction	T_f	$N \cdot m$	$4.2 \cdot 10^{-3}$
Maximum Current	$I_{\max}$	A	5.19
Minimum Current	$I_{\min}$	A	–5.19
Internal Gear Ratio	K_s	–	218.4^{-1}

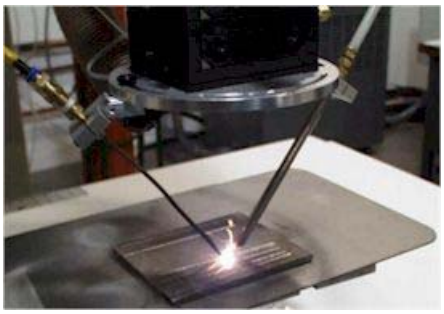

Figure 1: Laser Metal Deposition Manufacturing Process.

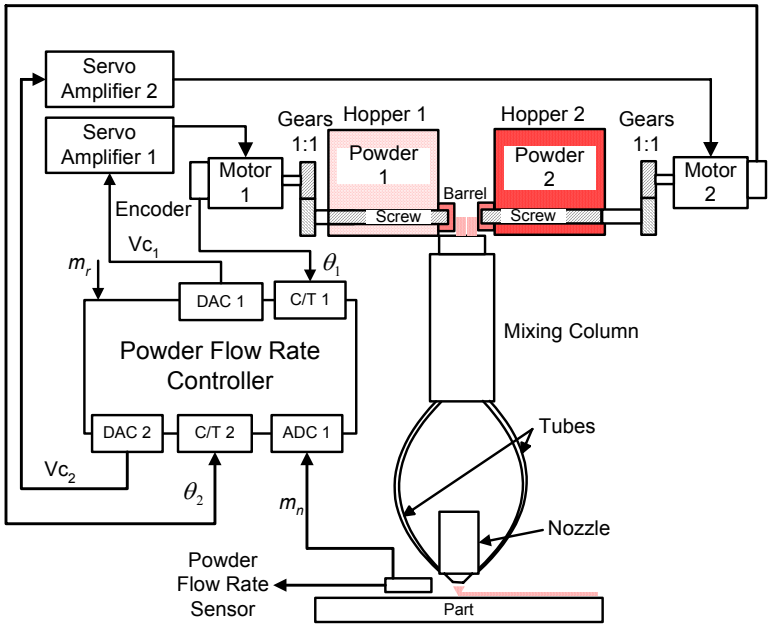

Figure 2: Powder Feeder System Schematic.

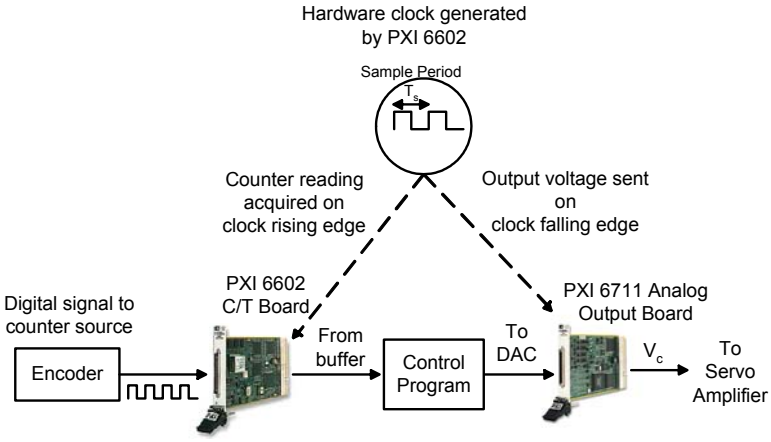

Figure 3: Control Loop Hardware Timing Scheme. C/T and Analog Board Pictures from www.ni.com.

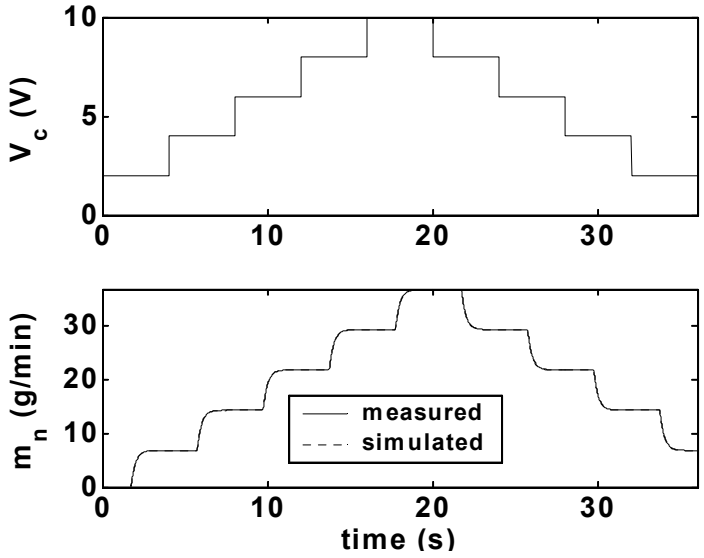

Figure 4: Model Validation Experimental Results for Step Inputs. Measured and Simulated Results are Nearly Identical.

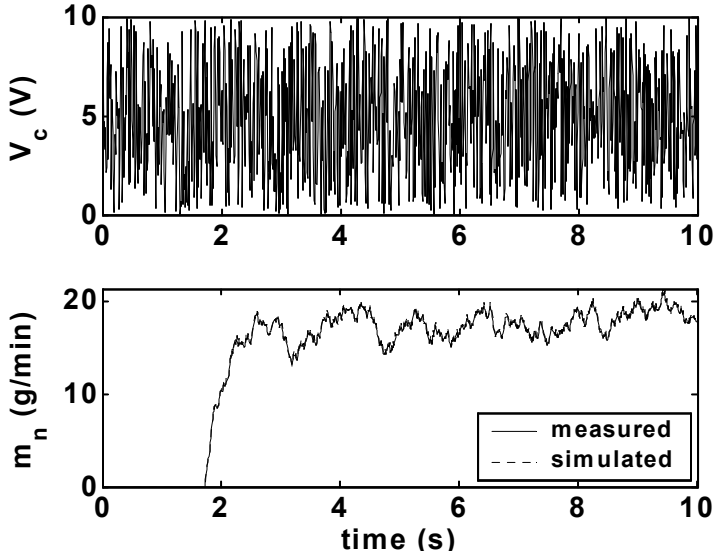

Figure 5: Model Validation Experimental Results for White Noise Input. Measured and Simulated Results are Nearly Identical.

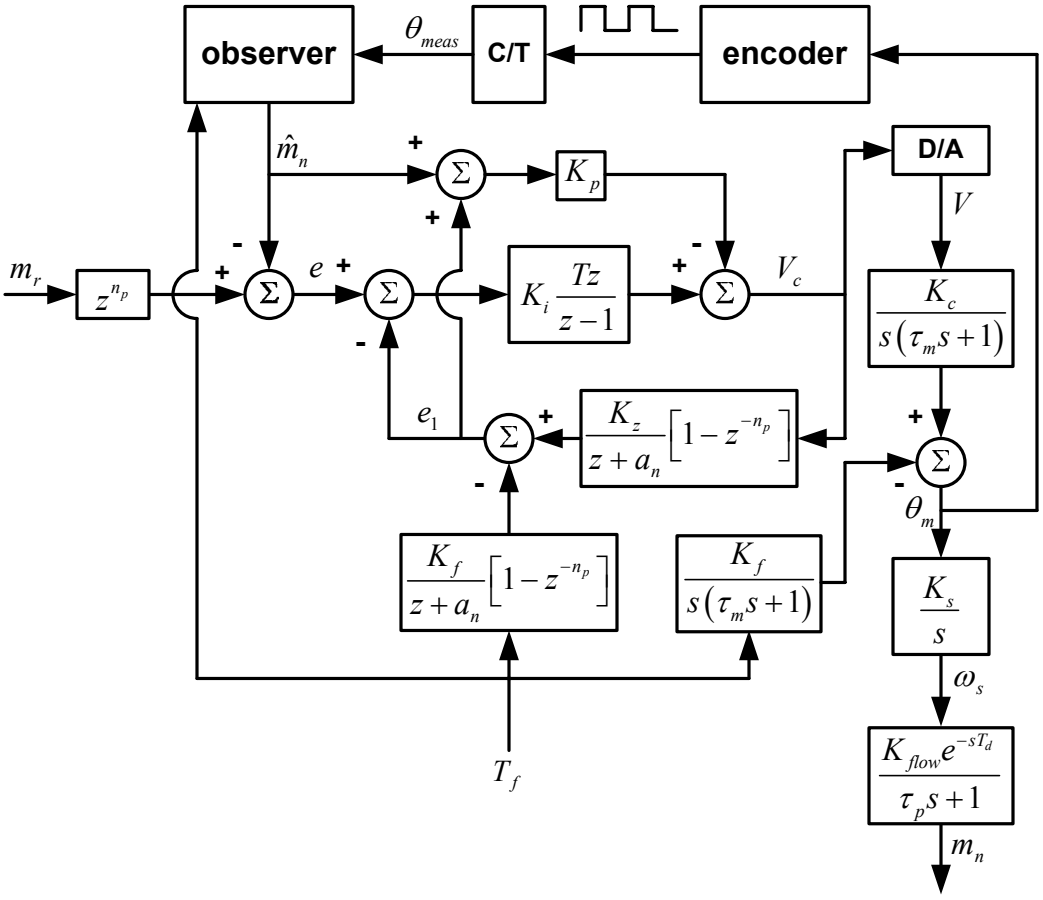

Figure 6: Closed–Loop System Schematic with Modified PI Controller Implemented in a SPCS.

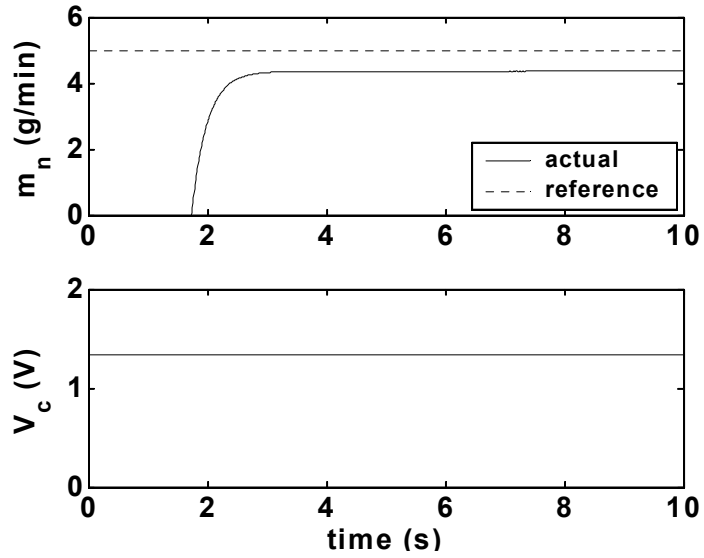

Figure 7: Experimental Results for Constant Command Voltage (m_r = 5 *g*/*min*).

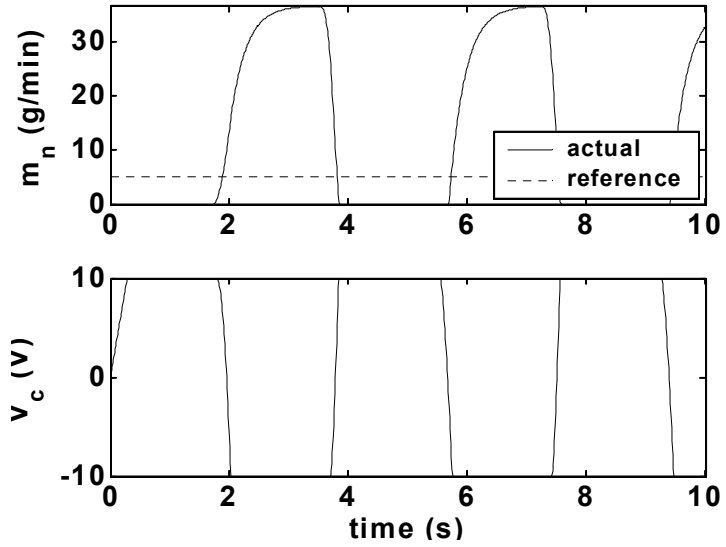

Figure 8: Experimental Results for Controller not Implemented in SPCS (m_r = 5 *g*/*min*).

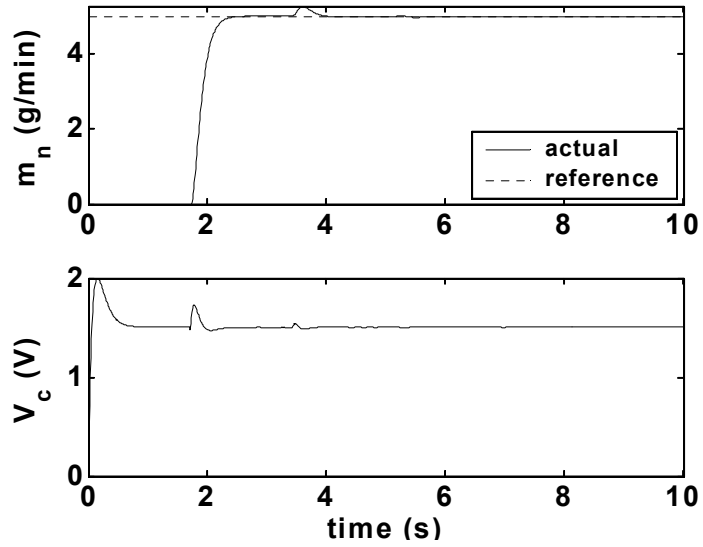

Figure 9: Experimental Results for Controller Implemented in SPCS (m_r = 5 *g*/*min*).

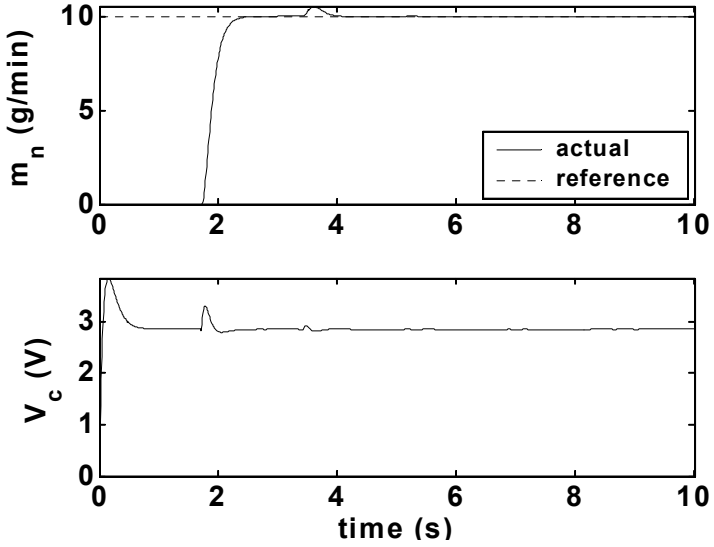

Figure 10: Experimental Results for Controller Implemented in SPCS (m_r = 10 *g*/*min*).

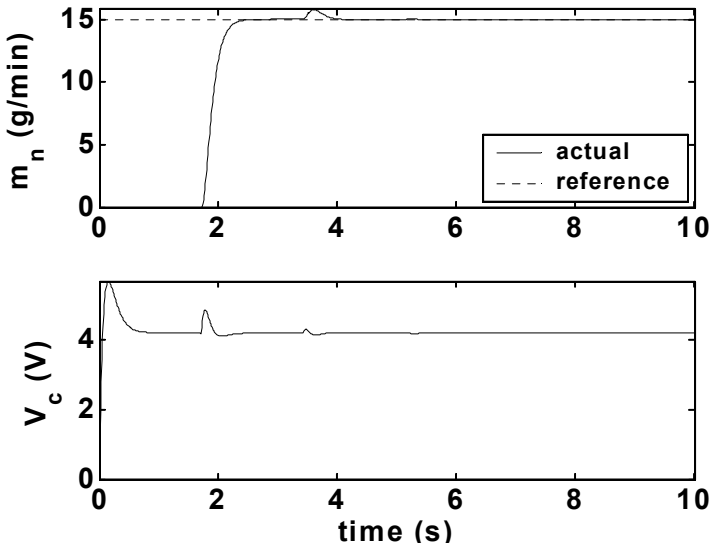

Figure 11: Experimental Results for Controller Implemented in SPCS (m_r = 15 *g*/*min*).

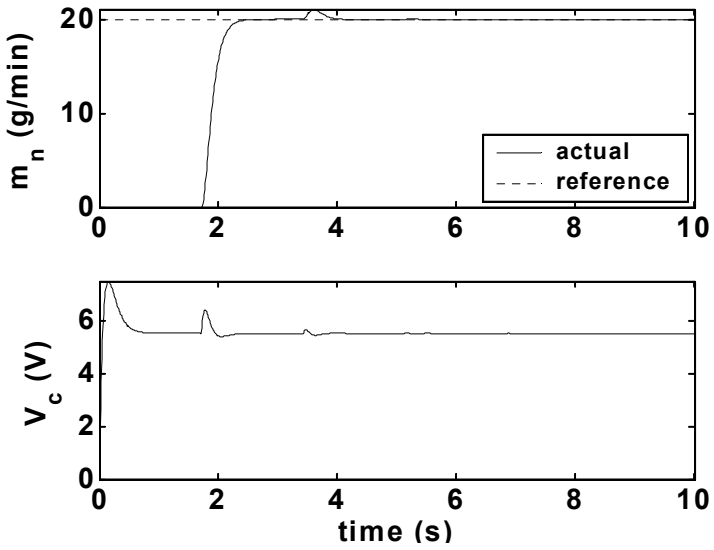

Figure 12: Experimental Results for Controller Implemented in SPCS (m_r = 20 *g*/*min*).

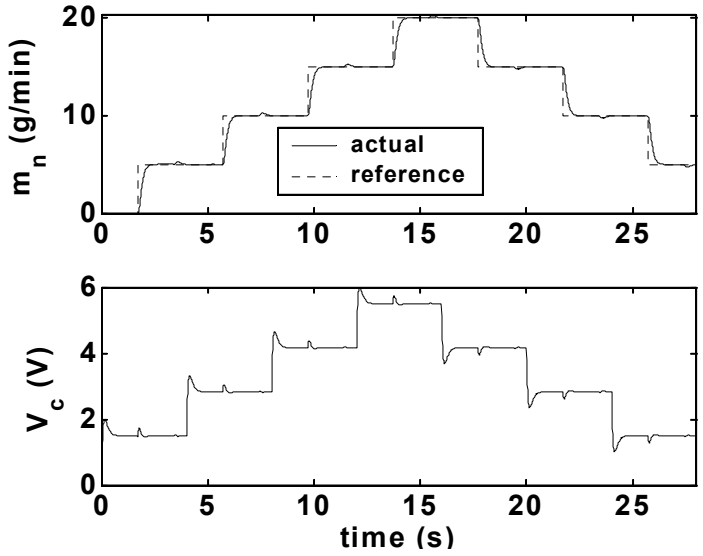

Figure 13: Experimental Results for Controller Implemented in SPCS (multiple step references).